Low-Spurious Multiformat Microwave Signal Generation Based on an Actively Mode-Locked Dual-Loop Optoelectronic Oscillator

Changlong Du, Shifeng Liu, Li Yang, Mingzhen Liu, Liangzun Tang, Hao Chen, Xiangqian Xu, Wentong Chen, and Shilong Pan, *Fellow, IEEE*

***Abstract*—A novel photonic approach for the generation of multiformat microwave signals with low-spurious components is proposed and experimentally demonstrated, based on an actively mode-locked dual-loop optoelectronic oscillator (OEO). In this scheme, a low-frequency electrical signal is injected into the Mach–Zehnder modulator (MZM) to dynamically control the net gain of the OEO cavity. When the modulation frequency is set to an integer multiple of the cavity's free spectral range (FSR), harmonic mode locking is realized, enabling flexible waveform generation. By tailoring the waveform format of the injected signal, the OEO is capable of generating a diverse set of microwave signal types, including single-tone carriers, pulse trains, rectangular waveforms, staggered pulses, and pulse-coded signals. To suppress undesired longitudinal modes and mitigate supermode noise, a dual-loop architecture exploiting the Vernier effect is employed, significantly enhancing spectral purity. In proof-of-concept experiments, a single-tone signal at 10.8 GHz with a side-mode suppression ratio of 82 dB is achieved, corresponding to a 55-dB improvement compared to a single-loop configuration. Microwave pulse trains with a 603-kHz repetition rate are also generated under 13th-order harmonic mode locking, exhibiting phase noise levels better than −140 dBc/Hz at a 10-kHz offset and a supermode suppression ratio exceeding 80 dB. This represents an enhancement of more than 70 dB in supermode noise suppression relative to the single-loop case. The proposed architecture provides a compact, low noise, and adjustable solution for high-purity microwave waveform generation, with potential applications in radar, wireless communications, and electronic warfare systems.**

***Index Terms*—Active mode locking, dual loop, multiformat signal, optoelectronic oscillators (OEOs), phase noise, spurious suppression.**

I. Introduction

LOW-PHASE-NOISE multiformat signals play a critical role in modern radar and communication systems by enhancing interference suppression, improving target detection accuracy, and enabling greater system flexibility and adaptability [1], [2], [3], [4]. Conventional microwave signal generation techniques, such as direct digital synthesis (DDS) and voltage-controlled oscillators (VCOs), are typically constrained by limited carrier frequency ranges, narrow bandwidth, and poor phase noise performance limitations that hinder their application in next-generation high-frequency microwave systems [5], [6]. Microwave photonic technologies have emerged as promising alternatives, offering broad bandwidth, high carrier frequencies, and inherent immunity to electromagnetic interference [7]. Various photonic schemes for multiformat microwave signal generation have been proposed [1], [2], [8], [9]. For instance, in [1], a dual-polarization Mach–Zehnder modulator (DP-MZM) is used to create an optical frequency comb and modulate it using a baseband signal to produce multiformat microwave signals via a photodetector (PD). In [8], amplitude, phase, and frequency-shift keying formats are implemented by adjusting drive signals and dc biases of a dual-parallel Mach–Zehnder modulator (MZM). In [9], a dual-polarization quadrature phase shift keying (DP-QPSK) modulator is adopted to enable the generation of dual-band, dual-chirp, and phase-coded microwave signals through heterodyne mixing, supporting flexible waveform synthesis. However, in these approaches, the phase noise performance of the generated signals is primarily constrained by that of the externally injected microwave sources, whose inherent phase noise degrade the overall signal purity.

Optoelectronic oscillators (OEOs) offer a promising platform for high-quality microwave signal generation, owing to their exceptional phase noise performance and excellent frequency scalability [10], [11]. Over the years, extensive research has been devoted to improving single-frequency signal characteristics, including phase noise reduction [12], [13], [14], side-mode suppression enhancement [15], [16], and frequency tunability [17], [18], [19]. In addition to narrowband operation, the functionality of OEOs has been extended toward wideband waveform generation. Specifically, the development of Fourier-domain mode-locked (FDML) OEOs has enabled the synthesis of chirped waveforms with large time–bandwidth products, significantly enhancing radar range resolution [20], [21], [22], [23]. More recently, time-domain mode-locking techniques have been introduced, facilitating the generation of high-repetition-rate microwave pulse trains with short durations and excellent phase coherence [24], [25], [26], [27].

Received 23 May 2025; revised 4 July 2025; accepted 18 July 2025. Date of publication 29 July 2025; date of current version 26 November 2025. This work was supported in part by the National Key Research and Development Program of China under Grant 2022YFB2802704, in part by Jiangsu Funding Program for Excellent Postdoctoral Talent under Grant 2022ZB237, and in part by the National Natural Science Foundation of China under Grant 62271249 and Grant 62071226. *(Corresponding author: Shifeng Liu.)*

Changlong Du, Shifeng Liu, Li Yang, Mingzhen Liu, Liangzun Tang, Xiangqian Xu, Wentong Chen, and Shilong Pan are with the National Key Laboratory of Microwave Photonics, Nanjing University of Aeronautics and Astronautics, Nanjing 210016, China (e-mail: changlongdu@nuaa.edu.cn; sfliu_nuaa@nuaa.edu.cn; liyang_photonic@nuaa.edu.cn; liumingzhen@nuaa.edu.cn; lztang@nuaa.edu.cn; qz26235200@163.com; zq19811002@126.com; pans@nuaa.edu.cn).

Hao Chen is with Hangzhou Institute of Advanced Studies, Zhejiang Normal University, Hangzhou 311231, China.

Digital Object Identifier 10.1109/TMTT.2025.3591453

To further enhance the flexibility and functionality of OEO systems, increasing research efforts have been devoted to the generation of multiformat waveforms based on OEO architectures [3], [28], [29]. In [3], multiformat microwave waveform generation is achieved by incorporating a DP-QPSK modulator within the oscillation loop. The oscillation signal, which serves as the local signal, is achieved using the upper dual-parallel MZM (DP-MZM) of the DP-QPSK modulator in the x-polarization, while the multiformat signals are generated in the y-polarization by mixing the oscillation signal and a baseband waveform in the lower DP-MZM. However, this approach involves considerable complexity, and the generated signal may suffer from degraded amplitude and frequency stability due to polarization drift induced by environmental fluctuations. In [28], a reconfigurable optical waveform generator is employed with a carrier-suppressed single-sideband (CS-SSB) modulation scheme and FDML-OEO structure to generate diverse low-phase-noise signals such as linear-chirp, frequency-hopping, and phase-coded waveforms. However, its implementation is costly and intricate. In [29], a simplified OEO configuration achieves waveform reconfigurability by modulating the loop gain via bias signals applied to the MZM. Although various waveform types were demonstrated, including sinusoidal signals, pulse trains, and rectangular waves, this bias-modulation approach increases system complexity and imposes limitations on the modulation frequency, thereby restricting the generation of higher repetition rate waveforms. Moreover, the use of a wideband RF filter resulted in severe mode competition and limited side-mode suppression. Under harmonic mode-locking conditions, the associated supermode noise further degraded spectral purity and compromised the system's practical applicability. The presence of supermode noise also reduced the stability of the generated signal, particularly in terms of spectral fluctuations and pulse amplitude variation.

In this work, we propose and experimentally demonstrate a dual-loop OEO architecture for low-phase-noise multiformat microwave signal generation based on the active mode-locking mechanism. By injecting low-frequency modulation waveforms into the RF port of the MZM, the net loop gain is dynamically controlled, enabling flexible generation of various signal formats, including single-tone carriers, microwave pulse trains, and rectangular waveforms with tunable duty cycles. This RF-driven modulation approach also contributes to a more compact and simplified system architecture. By leveraging the Vernier effect inherent to the dual-loop configuration, unwanted longitudinal modes are effectively suppressed, substantially reducing side mode and supermode noise. In the experiment, single-tone signals, pulse trains with repetition rates of 603 kHz, and rectangular waveforms with duty cycles of 20%, 50%, and 80% were successfully generated. The waveform flexibility further enables generation of pulse-coded formats through digital pattern modulation. Under harmonic mode locking, supermode suppression ratios exceeding 80 dB were achieved, owing to the dual-loop Vernier effect [26], [30], [31], which significantly enhances pulse stability. A phase noise level below −140 dBc/Hz at a 10-kHz offset was achieved for the generated microwave signal, demonstrating the low-phase-noise performance of the proposed system. This adjustable and compact approach provides an efficient solution for multiformat microwave waveform generation with low noise, making it a promising candidate for applications in advanced radar, secure communication, and electronic warfare systems.

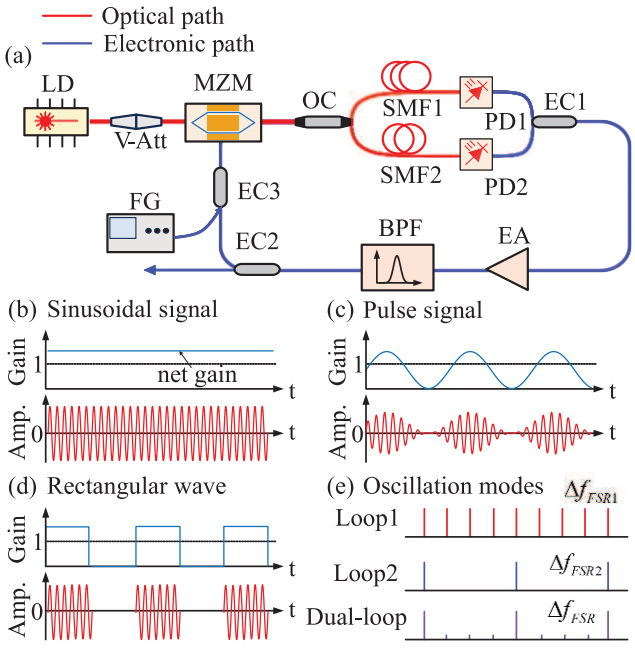

Fig. 1. Schematic of the proposed system for the generation of low-spurious multiformat microwave signals based on a dual-loop OEO. (a) System architecture of the dual-loop OEO. (b) Free-running operation without external modulation for single-tone microwave signal generation. (c) Sinusoidal waveform injection for generating microwave pulse trains via active mode locking. (d) Rectangular waveform injection for generating rectangular microwave waveforms with tunable duty cycles. (e) Illustration of the Vernier effect in the dual-loop configuration used to suppress unwanted longitudinal modes.

II. Principle and Analysis

The architecture of the proposed system is illustrated in Fig. 1(a). A continuous-wave laser diode (LD) serves as the optical source, delivering an output power of 20 dBm into the MZM. A variable attenuator (V-Att) is inserted to finely regulate the overall gain of the OEO loop. Inside the MZM, the optical carrier is modulated by a feedback microwave signal. The modulated optical signal is then evenly split by an optical coupler (OC) into two separate paths, each passing through single-mode fibers (SMFs) of different lengths. After passing through the SMFs, the signals are detected by high-speed PDs, converted into electrical signals, and subsequently combined and amplified via a low-noise electrical amplifier (EA) to compensate for loop attenuation. The amplified signal is passed through an electrical bandpass filter (BPF) to select the desired frequency components. The filtered signal is combined with a programmable microwave signal generated by a function generator (FG) using an electrical combiner (EC), and the resulting signal is fed to the RF port of the MZM, thereby completing the feedback loop. The OEO loop gain is dynamically controlled by adjusting the waveform of the externally

injected signal, enabling the generation of microwave signals with diverse formats. The dual-loop architecture exploits the Vernier effect to suppress spurious components, thereby significantly improving the spectral purity and overall signal quality. The resulting optical waveform at the MZM output can be described by

$$E_{\text{out}}(t) = E_0 \exp(j\omega_0 t) \cos\left\{\frac{\pi}{2V_\pi}\left[V_{\text{in}}(t) + V_{\text{FG}}(t) + V_{\text{DC}}\right]\right\} \tag{1}$$

where E_0 and ω_0 represent the amplitude and the angular frequency of the optical carrier, respectively. V_{DC} and V_π are bias voltage and half-wave voltage of the modulator, respectively. $V_{\text{in}}(t)$ corresponds to the microwave signal, which generated by the OEO, while $V_{\text{FG}}(t)$ is the signal generated by the FG. Therefore, the voltage of the electrical signal applied to the MZM after one complete round trip within the OEO loop can be expressed as

$$V_{\text{out}}(t) = V_{\text{ph}}\left\{1 + \cos\left[\frac{\pi}{V_\pi}(V_{\text{in}}(t) + V_{\text{FG}}(t) + V_{\text{DC}})\right]\right\} \tag{2}$$

where $V_{\text{ph}} = 0.5 G_{\text{A}} R \Re P_{\text{c}} \alpha$, in which G_{A} is the gain of the EA; $\Re$ and R are the responsivity and impedance of the PD, respectively; and α is the loss of the optical fiber. Therefore, the open-loop gain within the OEO cavity can be formulated as follows:

$$G = \left.\frac{dV_{\text{out}}}{dV_{\text{in}}}\right|_{V_{\text{in}}=0} = \left|-\frac{\pi V_{\text{ph}}}{V_\pi} \sin\left[\frac{\pi}{V_\pi}(V_{\text{FG}}(t) + V_{\text{DC}})\right]\right|. \tag{3}$$

As shown in (3), the gain of the OEO loop G is directly modulated by the electrical waveform applied to the MZM. By modifying the waveform format of the low-frequency modulation signal, real-time control over the temporal evolution of the loop gain can be achieved. In Fig. 1(b), the blue curve represents the time-varying loop gain, while the red curve shows the corresponding output of the OEO. When no external signal is injected, the gain remains static, and the OEO operates in a conventional free-running regime, generating a continuous-wave single-tone microwave output. Upon injecting a periodic sinusoidal waveform into the MZM, the loop gain is periodically modulated, as shown in Fig. 1(c). If the modulation frequency f_{FG} matches the free spectral range (FSR) of the OEO cavity, microwave energy accumulates at points satisfying the net gain condition over multiple iterations, producing a microwave pulse with a repetition rate equal to the modulation frequency. Similarly, injecting a rectangular microwave waveform into the MZM causes the OEO to generate a rectangular microwave signal, as shown in Fig. 1(d).

To suppress the side mode and supermode noise, a dual-loop configuration is employed. As shown in Fig. 1(e), the effective FSR can be described by the following expression:

$$\Delta f_{\text{FSR}} = N_1 \Delta f_{\text{FSR1}} = N_2 \Delta f_{\text{FSR2}} \tag{4}$$

where $\Delta f_{\text{FSR}i} = 1/\tau = c/nL_i$ ($i = 1$ or 2) is the FSR of a signal-loop OEO with a length of L_i, τ_i is the delay of the OEO loop, c is the speed of the light, Δf_{FSR} is the least common multiple of Δf_{FSR1} and Δf_{FSR2}, and N_1 and N_2 are the smallest integers satisfying (4). The unmatched modes are effectively suppressed, leading to a significant improvement in both the side-mode suppression ratio and the supermode suppression ratio.

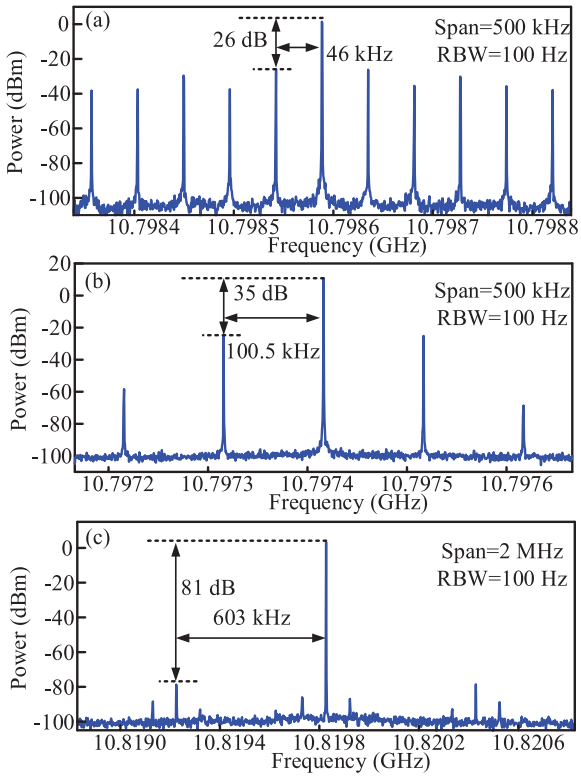

Fig. 2. Measured RF spectra of the OEO under different loop configurations. (a) Single-loop OEO with a 4.4-km fiber length. (b) Single-loop OEO with a 2-km fiber length. (c) Dual-loop OEO exhibiting enhanced side-mode suppression due to the Vernier effect.

III. Experimental Results

A proof-of-concept experiment was conducted using the setup illustrated in Fig. 1(a), where a continuous-wave (LD, E0069718) emitted light at a center wavelength of 1550 nm with an optical power of 20 dBm. A variable optical attenuator regulated the optical power entering the MZM, allowing precise control of the net gain within the OEO loop. The MZM (Fujitsu FTM7938), featuring a 3-dB bandwidth of 20 GHz, was used to modulate the oscillating microwave signal. Two SMF delay lines, with lengths of approximately 2 and 4.4 km, were employed to form the dual-loop cavity. The modulated optical signals were detected using two high-speed PDs (CETC44 GD45220R) with 3-dB bandwidths of 18 GHz. An electrical BPF centered at 10.8 GHz with a 3-dB bandwidth of 50 MHz was employed to select the oscillation frequency. To compensate for loop loss, a low-noise EA (Talent Microwave TLNA02G18G) offering a small-signal gain of 30 dB over the 2–18-GHz range was incorporated. The oscillating microwave signal was then divided by a broadband power splitter (2–18 GHz), combined with an externally injected signal via a wideband EC (DC-26 GHz), and fed back into the MZM to close the loop.

Initially, the FG was turned off, and the MZM was biased at quadrature point, enabling the OEO to operate in a

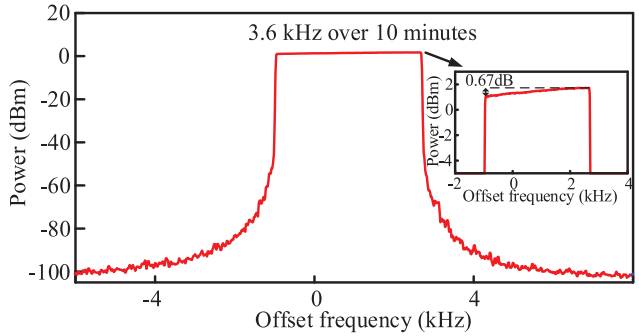

Fig. 3. Measured frequency and power stability of the generated RF signal from the dual-loop OEO over a 10-min interval using max-hold mode.

free-running single-tone oscillation mode. Fig. 2(a) and (b) displays the measured RF spectra of single-loop OEO using 4.4- and 2-km SMFs, respectively. Both measurements were conducted with a spectral span of 500 kHz and a resolution bandwidth (RBW) of 100 Hz. For the 4.4-km SMF, a mode spacing of 46 kHz and a side-mode suppression ratio of 26 dB were observed. When the SMF length was reduced to 2 km, the mode spacing increased to 100.5 kHz, and the side-mode suppression ratio improved to 35 dB. The narrow mode spacing associated with longer fiber lengths leads to strong gain competition and increased susceptibility to mode hopping, resulting in reduced side-mode suppression ratio and degraded spectral purity and signal stability. In contrast, Fig. 2(c) shows the spectrum of the signal generated by the dual-loop OEO, exhibiting a significantly improved side-mode suppression ratio of 81 dB. This corresponds to a 55-dB improvement compared to the single-loop configuration with a 4.4-km fiber. The measured mode spacing of 603 kHz matches the 13th harmonic of the 4.4-km loop and the 6th harmonic of the 2-km loop, demonstrating the effective suppression of unmatched longitudinal modes through the Vernier effect inherent in the dual-loop architecture.

As shown in Fig. 3, the stability of the microwave signal generated by the dual-loop OEO is evaluated using the max-hold mode of a spectrum analyzer over a 10-min interval. The frequency drift of the single-tone signal is observed to be 3.6 kHz, and as shown in the inserted zoomed-in plot, the corresponding power fluctuation is approximately 0.67 dB. These fluctuations are primarily attributed to environmental disturbances, such as thermal variations. Notably, no mode-hopping behavior was observed during the 10-min measurement period, indicating good longitudinal mode stability.

To enable active mode locking and generate microwave pulse signals, a sinusoidal waveform from the FG is applied to the MZM, with its frequency precisely tuned to the FSR of the dual-loop OEO. As shown in Fig. 4(a), when the frequency of the modulation sinusoidal signal is set to 603 kHz, a stable and equidistant microwave frequency comb with a smooth spectral envelope is generated. A magnified view over a 2-MHz span is presented in Fig. 4(b), with an RBW of 100 Hz. The measured signal-to-noise ratio exceeds 96 dB, which is attributed to the high quality factor of the OEO loop. It is worth noting that the active mode-locking operation exhibits high sensitivity

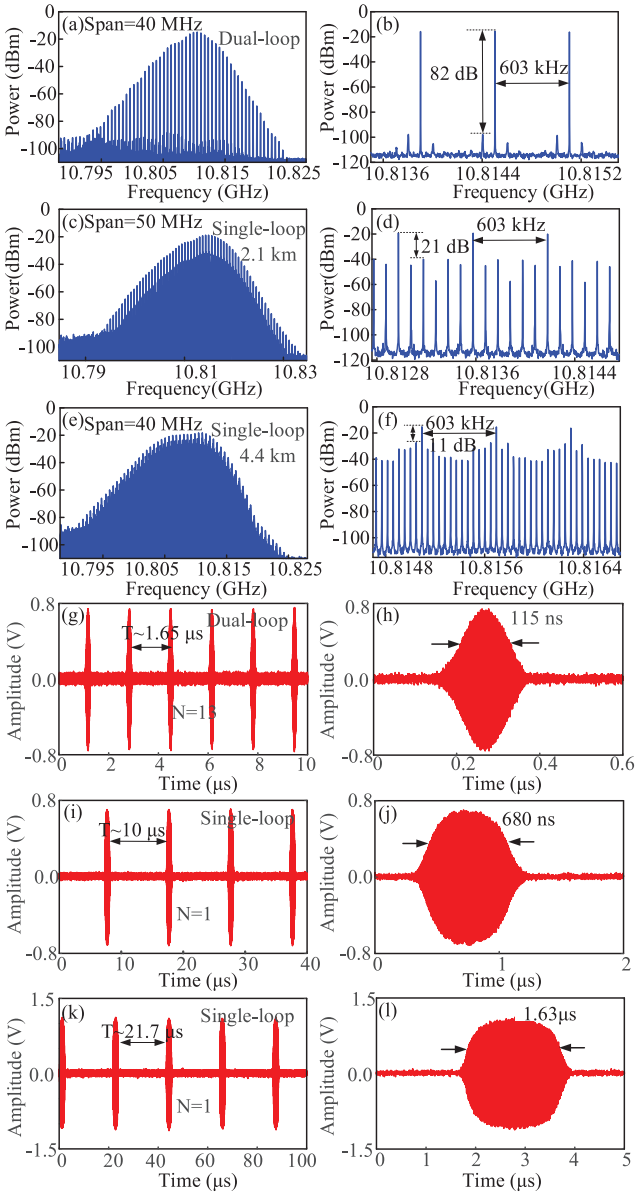

Fig. 4. Measured spectra and temporal waveforms of microwave pulse signals. (a) and (b) Spectra of the dual-loop OEO under 13th-order harmonic mode locking. (c) and (d) Spectra of the 2.1-km single-loop OEO under 13th-order harmonic mode locking. (e) and (f) Spectra of the 4.4-km single-loop OEO under 13th-order harmonic mode locking. (g) and (h) Waveform and FWHM of the pulse signal from the dual-loop OEO. (i) and (j) Waveform and FWHM from the 2.1-km single-loop OEO under fundamental mode locking. (k) and (l) Waveform and FWHM from the 4.4-km single-loop OEO under fundamental mode locking.

to the modulation frequency, with an effective locking range of approximately 603 kHz ± 100 Hz. When the modulation frequency deviates beyond this range, the mode-locking state gradually deteriorates, resulting in degraded signal stability. The frequency spacing between adjacent longitudinal modes matches the injection frequency of 603 kHz. Furthermore, due to the Vernier effect introduced by the dual-loop configuration, unwanted longitudinal modes are effectively suppressed. The measured supermode suppression ratio reaches 82 dB. For comparison, Fig. 4(c) and (d) presents the spectral characteristics of a 13th-order harmonic mode-locked single-loop OEO

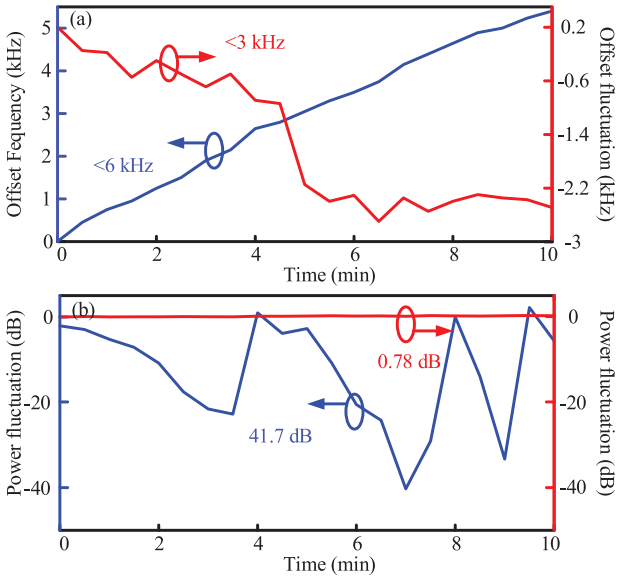

Fig. 5. Measured (a) frequency and (b) power stability of the microwave signal under 13th-order harmonic mode locking. Results are shown for the single-loop OEO (blue) and the dual-loop OEO (red).

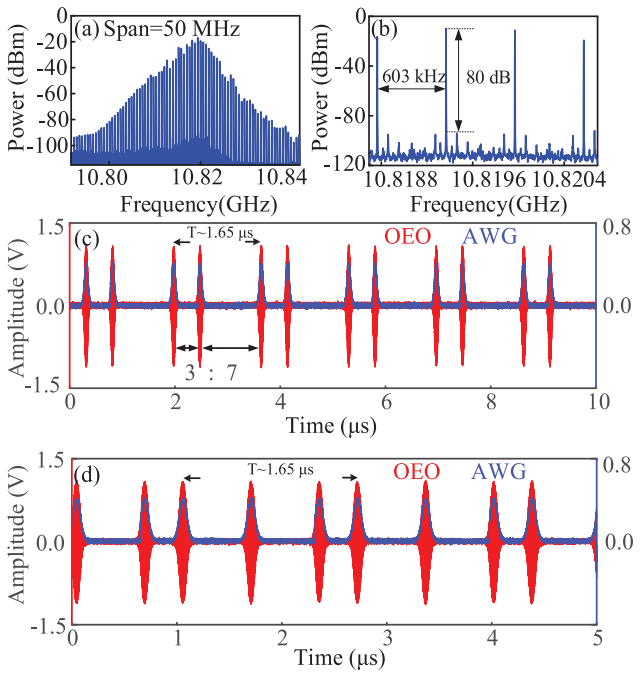

Fig. 6. (a) and (b) Measured spectra of the staggered pulse signal based on dual-loop OEO. (c) and (d) Temporal waveforms of the generated staggered pulse signal.

with a 2.1-km fiber. Although a relatively smooth envelope is observed, residual side modes remain visible and the measured supermode suppression ratio drops to 21 dB. Fig. 4(e) and (f) corresponds to a longer single-loop configuration with 4.4 km of fiber, where spurious sidebands become more pronounced and the supermode suppression ratio further decreases to 11 dB. These results verify that the dual-loop configuration improves the supermode suppression ratio by up to 70 dB compared with a single-loop design. The temporal waveform of the generated pulse signal is shown in Fig. 4(g), with a pulse period of 1.65 μs corresponding to the inverse of the 603-kHz modulation frequency. The measured full-width at half-maximum (FWHM) is approximately 115 ns, as illustrated in Fig. 4(h). Fig. 4(i) and (j) depicts the pulse waveform and FWHM of the single-loop OEO with 2.1-km fiber under fundamental mode locking, respectively. A wider pulsewidth of 680 ns is observed. Similarly, the pulse profile and FWHM under fundamental mode locking in the 4.4-km single-loop OEO are presented in Fig. 4(k) and (l), revealing a pulsewidth of 1.63 μs. Under 13th-order harmonic mode locking, the pulse repetition interval is significantly compressed, resulting in a much narrower pulse. In pulse-Doppler radar applications, higher pulse repetition frequency (PRF) and shorter pulses contribute to improved velocity resolution and target discrimination accuracy [26].

The frequency and power stability of microwave pulses generated under 13th-order harmonic mode locking were evaluated for both single- and dual-loop OEO configurations. A single-frequency component within the microwave frequency comb is selected for tracking monitoring over a 10-min interval, with measurements taken every 30 s. As illustrated in Fig. 5(a) and (b), both configurations maintain frequency drift within a few kilohertz. However, the power stability shows a marked difference. The single-loop OEO exhibits a power fluctuation of 41.7 dB, while the dual-loop configuration limits this drift to just 0.78 dB. These results indicate that supermode noise, arising from mode competition that triggers mode hopping, leads to significant power instability in the single-loop configuration. In contrast, the dual-loop configuration significantly improves power stability during harmonic mode locking by effectively suppressing undesired longitudinal modes through the Vernier effect. This improvement is attributed to effective supermode noise suppression in the dual-loop OEO. In harmonic mode locking, multiple mode groups can oscillate within the filter bandwidth, leading to mode competition and instability in single-loop structures. The dual-loop configuration introduces a Vernier effect that enlarges the effective FSR of the loop, thereby suppressing unwanted longitudinal modes. This selective oscillation allows only the desired mode to dominate, significantly enhancing the spectral purity and power stability of the generated signal.

In pulse-Doppler radar systems, a fixed PRF inherently limits the maximum unambiguous range ($R_{\max}$) and maximum unambiguous velocity ($V_{\max}$), which are governed by the well-known tradeoff [32]

$$R_{\max} = \frac{c}{2\mathrm{PRF}} \tag{5}$$

$$V_{\max} = \frac{\lambda}{4}\mathrm{PRF} \tag{6}$$

where c is the speed of light and λ is the radar wavelength. To address the inherent tradeoff between the maximum unambiguous range and velocity in pulse-Doppler radar systems, staggered microwave pulses with programmable and nonuniform pulse repetition intervals provide an effective solution. This technique slightly compromises range resolution but significantly extends the unambiguous velocity limit. It

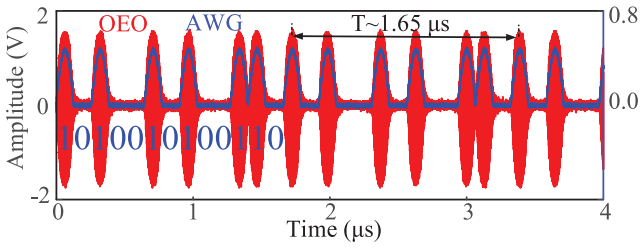

Fig. 7. Measured time-domain waveforms of the encoded microwave pulse trains generated by the dual-loop OEO using a binary coding sequence of "1010010100110."

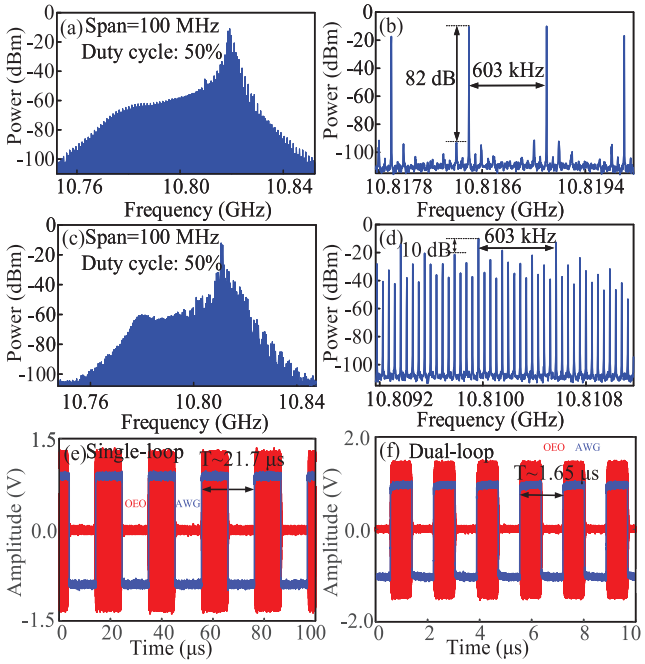

Fig. 8. Measured the spectra of the generated rectangular microwave waveforms with a duty cycle of 50% form 13th-order harmonic mode-locking OEO based on either (a) and (b) dual-loop or (c) and (d) single-loop architecture and temporal of the generated signal based on (e) fundamental and (f) harmonic mode-locking OEO.

also helps to mitigate range–Doppler ambiguity and enhances target detection performance [33]. Therefore, staggered pulse waveforms are well suited for high-resolution imaging and velocity-resolved radar applications. In this work, the FG is programmed to produce a full-wave driving signal with a base PRF of 603 kHz, featuring two amplitude peaks per cycle at a temporal ratio of 3:7, as shown by the blue curve in Fig. 6(c). According to (3), the OEO's loop gain exceeds unity only at these amplitude peaks, resulting in the generation of staggered double-pulse signals. According to (3), the OEO loop gain exceeds unity only at these peaks, thereby enabling the generation of staggered double-pulse waveforms. The corresponding spectrum is presented in Fig. 6(a), with a magnified view in Fig. 6(b). The achieved supermode suppression ratio of 80 dB validates the high spectral purity of the generated waveform. The red trace in Fig. 6(c) shows the measured time-domain waveform, exhibiting two pulses within a 1.65-μs period, aligned to the 3:7 time ratio. By modifying the driving waveform to include three amplitude peaks per cycle, as depicted in Fig. 6(d), the OEO successfully produces staggered triple-pulse signals, as shown by the red curve in the same figure. These results demonstrate the programmability of the proposed scheme in generating multipulse waveforms with tunable intraperiod timing, offering enhanced flexibility for advanced radar waveform design and multi-PRF synthesis.

The pulse-coded microwave waveform significantly enhances radar system performance by enabling high range resolution through pulse compression, increasing energy efficiency without requiring high peak power, and improving target detection under low signal-to-noise ratio. In addition, the coded structure provides inherent resilience to interference and allows for signal encryption and identification in secure applications [34], [35], [36]. This architecture further supports flexible waveform reconfiguration through pulse position encoding. As a proof-of-concept, a full-wave modulation signal is amplitude-encoded using a 13-bit binary sequence ("1010010100110") at a repetition rate of 603 kHz. The blue waveform in Fig. 7 represents the encoded signal applied to the MZM. When the instantaneous amplitude is "1," the loop gain exceeds the oscillation threshold, enabling pulse generation. In contrast, when the amplitude is "0," the loop remains below threshold, and no oscillation occurs. The resulting red trace in Fig. 7 shows a pulse train that accurately reflects the encoded binary pattern, with a repetition period of 1.65 μs. By simply modifying the binary sequence, arbitrary pulse positions within each cycle can be defined. This encoding-based control mechanism enhances the system's waveform agility and anti-jamming capability, making it well suited for advanced applications in secure radar and communication systems.

When a rectangular waveform with a repetition rate of 603 kHz is applied to the MZM, as shown by the blue curve in Fig. 8(f), the OEO operates in a gain-switching regime, generating microwave signals with rectangular temporal profiles. According to (3), oscillation occurs only when the loop gain exceeds unity. As a result, the duty cycle of the generated microwave waveform directly follows that of the injected rectangular signal, allowing precise control via input waveform adjustments. Fig. 8(a) and (b) shows the spectral profiles of rectangular microwave signals generated by a 13th-order harmonic mode-locked OEO in a dual-loop configuration with a 50% duty cycle. The observed mode spacing of 603 kHz aligns with the external modulation frequency, and a supermode suppression ratio of 82 dB is achieved. In contrast, Fig. 8(c) and (d) depicts the spectra obtained from a single-loop OEO under the same conditions, with the supermode suppression ratio reduced to just 10 dB. This comparison highlights the superior supermode noise suppression capability of the dual-loop configuration. The corresponding time-domain waveform for the dual-loop case is shown in Fig. 8(f), exhibiting a pulse repetition period that is 1/13 of that observed under fundamental mode locking in the single-loop structure, as depicted in Fig. 8(e). The blue curve in Fig. 8(e) illustrates a 46-kHz square wave with a 50% duty cycle, whose envelope matches

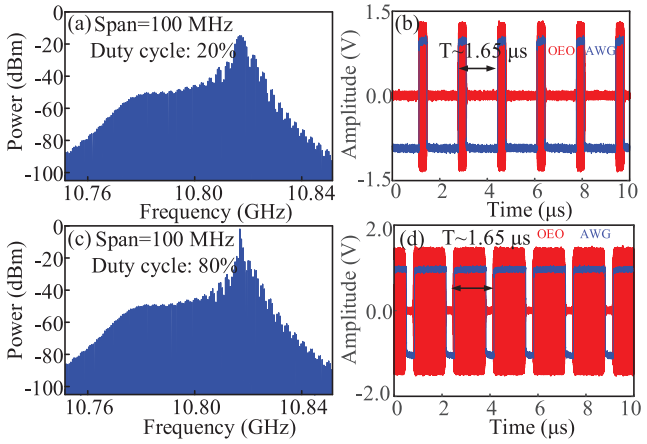

Fig. 9. Measured spectra and time-domain waveforms of the generated rectangular microwave signals with duty cycles of (a) and (b) 20% and (c) and (d) 80%.

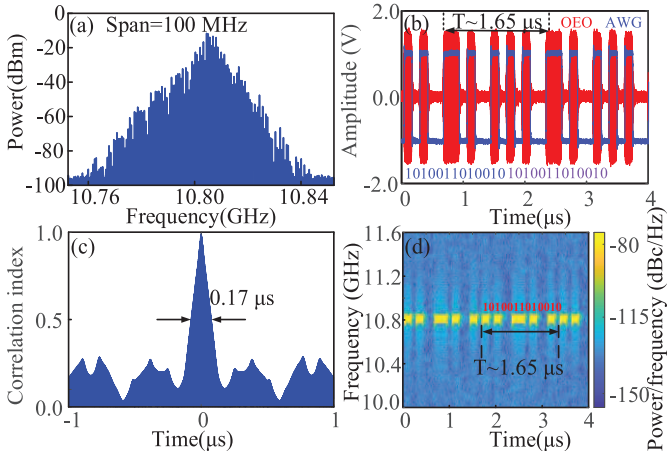

Fig. 10. (a) Measured spectrum and (b) time-domain waveform of the generated pulse-coded microwave signal. (c) Autocorrelation trace of the waveform shown in (b), indicating temporal resolution. (d) STFT spectrogram corresponding to the data in (b), confirming the encoded sequence.

the generated microwave pulse train under fundamental mode locking.

By varying the duty cycle of the injected rectangular waveform, rectangular microwave signals with different temporal widths can be synthesized. Fig. 9(a) and (b) displays the spectral and temporal responses of the signal with a 20% duty cycle, while Fig. 9(c) and (d) corresponds to an 80% duty cycle. The blue curves in Fig. 9(b) and (d) show the injected low-frequency rectangular signals with a repetition rate of 603 kHz and duty cycles of 20% and 80%, respectively, which directly determine the temporal profiles of the generated microwave pulses. These results confirm the system's reconfigurability in duty cycle control. Furthermore, pulse-coded microwave waveforms can be generated by encoding the low-frequency rectangular drive with a binary sequence. As a demonstration, a 13-bit binary code "1010011010010" with a repetition rate of 603 kHz is used. Fig. 10(a) and (b) presents the corresponding spectrum and time-domain waveform, respectively. In Fig. 10(b), the blue curve represents the

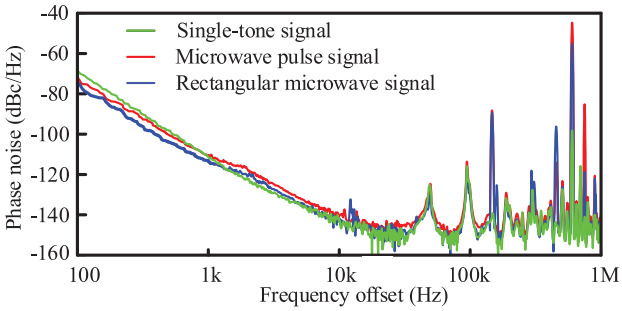

Fig. 11. Measured single-sideband phase noise of the generated microwave signals centered at 10.8 GHz, including the single-tone signal, microwave pulse signal, and rectangular microwave signal.

injected pulse-coded rectangular waveform, which governs the envelope of the generated microwave signal. Fig. 10(c) shows the autocorrelation of the output signal, yielding a compressed pulse with an FWHM of approximately 0.17 μs, indicating high temporal resolution. The time–frequency spectrogram, derived via short-time Fourier transform (STFT), is presented in Fig. 10(d), clearly revealing the encoded sequence and confirming the periodicity of 1.65 μs, consistent with the input signal.

Fig. 11 presents the phase noise performance of the generated multiformat microwave signals. At a 10-kHz offset, the single-tone signal achieves a phase noise level of −142 dBc/Hz, contributing to enhanced measurement precision and improved target resolution in radar systems. Furthermore, the phase noise levels for both microwave pulse signal and rectangular microwave signal remain below −140 dBc/Hz at the same frequency offset. These results verify the system's suitability for high-precision range and velocity measurements in pulse-Doppler radar applications.

IV. Conclusion

In conclusion, we have proposed and experimentally demonstrated an adjustable photonic architecture for generating low-spurious multiformat microwave signals based on an actively mode-locked dual-loop OEO. By shaping the waveform of the injected low-frequency electrical signal applied to the MZM, the loop gain is selectively modulated, enabling the generation of various signal formats, including single-tone, pulsed, rectangular, staggered, and coded waveforms. The adoption of a dual-loop configuration, leveraging the Vernier effect, plays a pivotal role in suppressing undesired longitudinal modes and enhancing spectral purity. Specifically, the side-mode suppression ratios of single-tone signals and the supermode noise in harmonic mode-locked pulse generation are both significantly reduced. Compared to a conventional single-loop OEO, the proposed system achieves an improvement of more than 50 dB in side-mode suppression ratio and over 70-dB enhancement in supermode noise suppression. All generated signals exhibit excellent phase noise performance, with measured levels below −140 dBc/Hz at a 10-kHz offset. Benefiting from low phase noise, minimized spurious components, and high waveform agility, the proposed OEO-based system provides a compact, high-performance

solution for advanced microwave signal synthesis. It is highly promising for deployment in next-generation radar systems, high-capacity wireless communication, and electronic warfare platforms.

REFERENCES

[1] L. Wang et al., "Photonic generation of multiband and multi-format microwave signals based on a single modulator," *Opt. Lett.*, vol. 45, no. 22, pp. 6190–6193, Nov. 2020.

[2] W. Gou et al., "Photonic-based multiformat signal generator with dispersion immunity for multichannel transmission," *IEEE Trans. Microw. Theory Techn.*, vol. 72, no. 2, pp. 1280–1289, Feb. 2024.

[3] Y. Chen, S. Liu, and S. Pan, "Multi-format signal generation using a frequency-tunable optoelectronic oscillator," *Opt. Exp.*, vol. 26, no. 3, pp. 3404–3420, Feb. 2018.

[4] T. Hao et al., "Recent advances in optoelectronic oscillators," *Adv. Photon.*, vol. 2, no. 4, Oct. 2020, Art. no. 044001.

[5] Y. Xu, T. Jin, H. Chi, S. Zheng, X. Jin, and X. Zhang, "Photonic generation of dual-chirp waveforms with improved time-bandwidth product," *IEEE Photon. Technol. Lett.*, vol. 29, no. 15, pp. 1253–1256, Aug. 1, 2017.

[6] Q. Cen et al., "Rapidly and continuously frequency-scanning optoelectronic oscillator," *Opt. Exp.*, vol. 25, no. 2, pp. 635–643, Jan. 2017.

[7] D. Marpaung, J. Yao, and J. Capmany, "Integrated microwave photonics," *Nature Photon.*, vol. 13, no. 2, pp. 80–90, Feb. 2019.

[8] S. Zhu, J. Feng, K. Zhai, Y. Zhang, N. Zhu, and E. Y. Pun, "Multi-format switchable microwave signal generation based on optical domain modulation," in *Proc. IEEE Region 10 Conf. (TENCON)*, Nov. 2022, pp. 1–3.

[9] X. Fan et al., "Photonic-assisted multi-format dual-band microwave signal generator without background noise," *Opt. Exp.*, vol. 31, no. 11, pp. 18346–18355, May 2023.

[10] H. Peng, N. Liu, and Z. Chen, "Suppression of AM to PM conversion induced phase noise in Brillouin optoelectronic oscillator," in *Proc. Asia Commun. Photon. Conf. (ACP)*, Nov. 2019, pp. 1–3.

[11] K. Volyanskiy, Y. K. Chembo, L. Larger, and E. Rubiola, "Contribution of laser frequency and power fluctuations to the microwave phase noise of optoelectronic oscillators," *J. Lightw. Technol.*, vol. 28, no. 18, pp. 2730–2735, Sep. 2010.

[12] H. Peng et al., "Suppression of phase noise induced by optical interference in optoelectronic oscillators," in *Proc. 21st Optoelectron. Commun. Conf. (OECC) Held Jointly Int. Conf. Photon. Switching (PS)*, Jul. 2016, pp. 1–3.

[13] Y. Wang et al., "Highly improved side mode suppression ratio and a low phase noise optoelectronic oscillator," *Appl. Opt.*, vol. 61, no. 15, pp. 4602–4609, May 2022.

[14] M. Liu, S. Liu, L. Yang, C. Du, H. Liu, and S. Pan, "Improving the quality of arbitrary periodic waveform via injection-locking of an optoelectronic oscillator," *IEEE Trans. Microw. Theory Techn.*, vol. 72, no. 11, pp. 6678–6685, Nov. 2024.

[15] A. Banerjee, L. Aguiar Dantas de Britto, and G. Mendes Pacheco, "Analysis of injection locking and pulling in single-loop optoelectronic oscillator," *IEEE Trans. Microw. Theory Techn.*, vol. 67, no. 5, pp. 2087–2094, May 2019.

[16] S. F. Liu, C. L. Du, L. Yang, M. Z. Liu, Z. Z. Tang, and S. L. Pan, "Coherent dual-frequency signal generation in an optoelectronic oscillator," *Opt. Lett.*, vol. 48, no. 11, pp. 2921–2924, May 2023.

[17] H. Peng et al., "Wideband tunable optoelectronic oscillator based on the deamplification of stimulated Brillouin scattering," *Opt. Exp.*, vol. 25, no. 9, pp. 10287–10305, May 2017.

[18] H. Tang, Y. Yu, Z. Wang, L. Xu, and X. Zhang, "Wideband tunable optoelectronic oscillator based on a microwave photonic filter with an ultra-narrow passband," *Opt. Lett.*, vol. 43, no. 10, pp. 2328–2331, May 2018.

[19] H. Peng et al., "Tunable DC-60 GHz RF generation utilizing a dual-loop optoelectronic oscillator based on stimulated Brillouin scattering," *J. Lightw. Technol.*, vol. 33, no. 13, pp. 2707–2715, Jul. 1, 2015.

[20] T. Hao et al., "Breaking the limitation of mode building time in an optoelectronic oscillator," *Nature Commun.*, vol. 9, no. 1, p. 1839, May 2018.

[21] T. Hao, J. Tang, N. Shi, W. Li, N. Zhu, and M. Li, "Dual-chirp Fourier domain mode-locked optoelectronic oscillator," *Opt. Lett.*, vol. 44, no. 8, pp. 1912–1915, Apr. 2019.

[22] Y. Wang, X. Li, J. Zhang, and J. Wo, "Spurious level and phase noise improved Fourier domain mode-locked optoelectronic oscillator based on a self-injection-locking technique," *Opt. Exp.*, vol. 29, no. 5, pp. 7535–7543, Mar. 2021.

[23] T. Hao, J. Tang, W. Li, N. Zhu, and M. Li, "Tunable Fourier domain mode-locked optoelectronic oscillator using stimulated Brillouin scattering," *IEEE Photon. Technol. Lett.*, vol. 30, no. 21, pp. 1842–1845, Nov. 1, 2018.

[24] B. Yang et al., "Active mode-locking optoelectronic oscillator," *Opt. Exp.*, vol. 28, no. 22, pp. 33220–33227, Oct. 2020.

[25] C. Lin, Y. Wang, A. Wang, J. Zhang, and X. Peng, "Active mode lock optoelectronic oscillator based on the simulated Brillouin scattering effect," *Appl. Opt.*, vol. 61, no. 24, pp. 7071–7077, Aug. 2022.

[26] Z. Zeng et al., "Harmonically mode-locked optoelectronic oscillator with ultra-low supermode noise," *Opt. Laser Technol.*, vol. 151, Jul. 2022, Art. no. 108036.

[27] Y. Li, M. Wang, J. Zhang, H. Mu, C. Wang, and F. Yan, "Supermode noise suppression with polarization-multiplexed dual-loop for active mode-locking optoelectronic oscillator," *Opt. Lett.*, vol. 47, no. 2, pp. 413–416, 2022.

[28] Y. Chen, P. Zuo, and T. Shi, "Optoelectronic oscillator for arbitrary microwave waveform generation," *J. Lightw. Technol.*, vol. 39, no. 19, pp. 6033–6044, Oct. 2021.

[29] Z. Zeng et al., "Multi-format microwave signal generation based on an optoelectronic oscillator," *Opt. Exp.*, vol. 29, no. 19, pp. 30834–30843, Sep. 2021.

[30] X. S. Yao, L. Maleki, Y. Ji, G. Lutes, and M. Tu, "Dual-loop optoelectronic oscillator," in *Proc. IEEE Int. Freq. Control Symp.*, May 1998, pp. 545–549.

[31] D. Zhu, S. Pan, and D. Ben, "Tunable frequency-quadrupling dual-loop optoelectronic oscillator," *IEEE Photon. Technol. Lett.*, vol. 24, no. 3, pp. 194–196, Feb. 2012.

[32] D. Posada et al., "Staggered multiple-PRF ultrafast color Doppler," *IEEE Trans. Med. Imag.*, vol. 35, no. 6, pp. 1510–1521, Jun. 2016.

[33] Y. Zhang et al., "Actively mode-locked modulator-free optoelectronic oscillator for multi-functional microwave pulse generation," *J. Lightw. Technol.*, vol. 42, no. 19, pp. 6760–6766, Oct. 1, 2024.

[34] E. C. Farnett, G. H. Stevens, and M. Skolnik, "Pulse compression radar," in *Radar Handbook*, 2nd ed. New York, NY, USA: McGraw-Hill, 1990, ch. 2, pp. 10–11.

[35] S. R. Deiss, R. J. Douglas, A. M. Whatley, and W. Maass, "A pulse-coded communications infrastructure for neuromorphic systems," in *Pulsed Neural Networks*, W. Maass and C. M. Bishop, Eds., Cambridge, MA, USA: MIT Press, 1999, ch. 6, pp. 157–178.

[36] G. Kim and Y. Park, "LiDAR pulse coding for high resolution range imaging at improved refresh rate," *Opt. Exp.*, vol. 24, no. 21, pp. 23810–23828, Oct. 2016.